New Folder Name Photothermal Deflection

Application of Photothermal Deflection Spectroscopy to the Detection of Absorption in Mirrors

M. E. Taylor

Abstract

Photothermal lensing deflection spectroscopy and photothermal deformation deflection spectroscopy are investigated as means of quantifying mirror absorption. The development and testing of an absorption detector are discussed.

I. Introduction

When a laser beam is incident on a mirror, a small fraction of its power is absorbed by the mirror coating. An even smaller fraction is absorbed by the substrate material. The heat deposited in the mirror through the absorption process leads to thermal lensing and thermally-induced deformation of the mirror surface. Because of these effects, it would be preferable for LIGO interferometers to operate with mirrors having absorptions as low as a tenth of a part per million rather than the one to five part per million mirrors currently available. In order to develop mirrors with very low absorptions, it is first necessary to develop methods of reliably determining mirror absorption.

The most common method of estimating the absorption of interferometer cavity mirrors is to observe the decay of circulating power in the cavity when the input laser beam is obstructed. The total cavity losses due to transmission,

LIGO-T910026-00-R

scattering, and absorption are obtained from the time constant of this decay curve. The absorption is calculated by subtracting the transmission and scattering losses. This last step introduces large uncertainties when the absorption losses are relatively small in comparison to the transmission and scattering losses. As a result, this method of calculating absorption is not feasible for mirrors having small absorptions.

It was the objective of the development stage of this project to explore means of determining absorption from the thermal lensing and thermal deformation resulting from absorptive heating, and to construct and test a detector to do so.

II. Expected PLDS Signal

When a mirror is exposed to a high-power "pump" beam, it is heated non-uniformly and a gradient in the index of refraction, a lens, develops within the heated area. A low-power "probe" beam incident on the heated region is deflected by the thermal lens. The measurement of absorption by observation of this deflection is referred to as photothermal lensing deflection spectroscopy (PLDS).

Expressions relating deflection and absorption were derived by N. Amer, A. Boccara, D. Fournier, and W. Jackson in their publication "Sensitive Photothermal Deflection Technique for Measuring Absorption in Optically Thin Media.[1]" Assuming that absorption occurs on the surface of the substrate, equations (1)

and (2) may be used,

$$\phi = \left(\frac{dn}{dT}\right)\left(\frac{2Pr}{\omega\rho c\pi^2 a^4}\right)\left(e^{-(r/a)^2}\right)\left(1 - e^{-\alpha\ell}\right) \tag{1}$$

$$\phi = \left(\frac{dn}{dT}\right)\left(\frac{P}{k\pi^2 r}\right)\left(1 - e^{-(r/a)^2}\right)\left(1 - e^{-\alpha\ell}\right) \tag{2}$$

where ϕ is the angular deflection, P is the incident pump beam power, ω is the angular modulation frequency of the pump beam, r is the separation between the intensity maxima of the pump and probe beams, a is the pump beam radius at $1/e$ intensity, $\alpha\ell$ is the absorption, ρc is the heat capacity per unit volume, dn/dT is the temperature coefficient of the index of refraction, and k is the coefficient of thermal conductivity.

Equation (1) is applicable when the period of the modulation is much less than the characteristic thermal diffusion time of the medium, given by equation (3).

$$\tau = \frac{\rho c}{k} a^2 \tag{3}$$

Equation (2) is applicable when the period of the modulation is much greater than the characteristic diffusion time. For a pump beam radius a of 200 μm and fused silica values of ρc of $2.08 \times 10^6\ Jm^{-3}K^{-1}$ and of k of 1.4 $Wm^{-1}K^{-1}$, equation (3) yields a time constant of 59 ms, which suggests that for typical pump radii equation (1) is valid at frequencies higher than 3 Hz and that equation (2) is valid at frequencies lower than 3 Hz.

For a pump beam radius a of 200 μm, an incident power P of $5W$, an absorption $\alpha\ell$ of 1 ppm, and fused silica values of ρc_p of 2.08 $\times$ 10^6 $Jm^{-3}K^{-1}$, of k of 1.4 $Wm^{-1}K^{-1}$, and of dn/dT of 1.28 $\times$ 10^{-5} K^{-1}, equations (1) and (2) yield maximum angular deflections on the order of 10^{-9} and 10^{-8} radians, at 20 Hz and 1 Hz, respectively.

Because equation (2) yields higher deflections for typical pump beam radii, it was decided that measurements would be taken in the frequency region corresponding to equation (2). The lineshape of equation (2) is shown in Figure 1.

III. Expected PDDS Signal

When a mirror is heated, as in the case of exposure to a pump beam, the heated region undergoes thermal expansion. In the bulk of the heated area, the expansion of each small region is constrained by neighboring material. Consequently, the surface deforms outward. A probe beam incident on the heated area is deflected by the deformation. The measurement of absorption by observation of this deflection is referred to as photothermal deformation deflection spectroscopy (PDDS). Expressions relating deflection and absorption were derived from formulae presented by M. Sparks in "Optical Distortion by Heated Windows in High-Power Laser Systems[2]" and by N. Amer, A. Boccara, D. Fournier, and W. Jackson in "Photothermal Deflection Spectroscopy and Detection.[3]" For a weakly absorbing medium such as fused silica, angular deflection ϕ is described

by equation (4),

$$\phi = \frac{(\nu+1)\mu\,\alpha\ell\,P}{2\pi r k}\left[\left[\int_0^{T_{0/2}}\left(e^{-\frac{2r^2}{w^2+8\kappa t}}-e^{\frac{-2r^2}{w^2}}\right)dt - \int_{T_{0/2}}^{T_0}\left(e^{\frac{-2r^2}{w^2+8\kappa t}}-e^{\frac{-2r^2}{w^2+8\kappa\left(t-T_{0/2}\right)}}\right)dt\right]^2 + \left[\int_{T_{0/4}}^{3T_{0/4}}\left(e^{\frac{-2r^2}{w^2+8\kappa t}}-e^{\frac{-2r^2}{w^2}}\right)dt - \int_0^{T_{0/4}}\left(e^{\frac{-2r^2}{w^2+8\kappa t}}-e^{\frac{-2r^2}{w^2+8\kappa\left(t+T_{0/2}\right)}}\right)dt - \int_{3T_{0/4}}^{T_0}\left(e^{\frac{-2r^2}{w^2+8\kappa t}}-e^{\frac{-2r^2}{w^2+8\kappa\left(t-T_{0/2}\right)}}\right)dt\right]^2\right]^{\frac{1}{2}} \quad (4)$$

where P is the incident pump beam power, r is the separation between intensity maxima of the pump and probe beams, w is the pump beam radius at $1/e^2$ intensity, T_0 is the modulation period, $\alpha\ell$ is the absorption, ν is the Poisson ratio, μ is the coefficient of linear thermal expansion, k is the coefficient of thermal conductivity, and κ is the diffusivity.

Because equation (4) is complicated in its analytical form, a program was written to calculate deflection for various input parameters. For a pump beam radius w of 280 μm, an incident power P of $5W$, an absorption $\alpha\ell$ of 1 ppm, a modulation period T_0 of 0.34 s, and fused silica values of ν of 0.17, of μ of 4.3 $\times$

$10^{-7}\ K^{-1}$, of k of 1.4 $Wm^{-1}K^{-1}$, and of κ of 7.92 $\times$ $10^{-7}\ m^2s^{-1}$, equation (4) yields a maximum deflection on the order of 10^{-9} radians.

The lineshape of equation (4) is shown in Figure 2.

IV. Detector Design

The detector is shown in its PLDS configuration in Figure 3 and in its PDDS configuration in Figure 4. It is composed primarily of an argon pump laser (514.5 nm), a helium-neon probe laser (632.8 nm), a helium-neon filter, an optical cavity, three quadrant photodiodes, an acousto-optic modulator, a square-wave generator, a lock-in amplifier, a piezo-actuated steering mirror, jitter-reduction electronics, cavity-locking electronics, and sundry mirrors, lenses, beamsplitters, and irises.

The pump beam, in passing through the acousto-optic modulator, is subjected to a square-wave power modulation. The modulated beam is incident on the cavity input mirror, which is optimized for transmission at the pump laser wavelength. The pump radius at the cavity input mirror is set by the mode-matching lenses. A beamsplitter directs a fraction of the modulated beam into the locking photodiode, which, in conjunction with the cavity-locking electronics, forces the cavity to resonate in its TEM00 mode. The probe beam is split into the signal beam and the reference beam, both of which are reflected off the piezo-actuated mirror. The reference beam passes through the cavity input mirror at a distance from the pump beam and then strikes the reference photodiode. An iris placed immediately in

front of the reference photodiode reduces the scattered pump light incident on the photodiode. The jitter-reduction system acts to suppress angular jitter common to both the reference and signal beams by adjusting the piezo-actuated mirror to maintain the reference beam's position on its photodiode. The signal beam is incident on the cavity input mirror at the location of the pump beam spot. When the detector is in its PLDS configuration, the signal beam passes through the cavity input mirror and into the signal photodiode. When the detector is in its PDDS configuration, the signal beam is reflected off the cavity input mirror and into the signal photodiode. An iris and a helium-neon filter, optimized for transmission at the probe laser wavelength, are placed imediately in front of the signal photodiode to reduce the scattered pump light incident on the photodiode. In both configurations, the output of the signal photodiode is fed into the lock-in amplifier and locked to the modulation frequency.

V. Noise and Noise Equivalent Signals

Electron shot noise originating in the signal photodiode introduces uncertainty into the PLDS and PDDS measurements. This uncertainty, derived from a discussion of shot noise by W. Hill and P. Horowitz in *The Art of Electronics*,[4] is given by equation (5),

$$\phi_{sn} = \frac{\pi}{8}\left[\frac{2e\Delta f}{i}\right]^{\frac{1}{2}}\frac{d}{\ell} \qquad (5)$$

where ϕ_{sn} is the apparent angular deflection of the beam due to shot noise current fluctuations, e is the electron charge, i is the current passing through the photodiode, Δf is the bandwidth, d is the signal beam diameter at the signal photodiode, and ℓ is the path length from the cavity input mirror to the signal photodiode.

For a current i of 1 mA, a diameter d of 2 mm, a path length ℓ of 0.25 m, and a bandwidth of 20 Hz, equation (5) yields a shot noise deflection limit on the order of 10^{-10} radians. Given the values assumed in earlier discussions of PLDS and PDDS, a deflection of that magnitude corresponds to a PLDS absorption of 0.01 ppm and a PDDS absorption of 0.1 ppm. Thus, detection of absorptions as low as 0.01 ppm and 0.1 ppm are theoretically possible with the PLDS and PDDS detector configurations, respectively.

A more realistic estimate of detector noise was determined by blocking the pump beam, modulating the probe beam, and observing the lock-in amplifier output. These measurements yielded PLDS and PDDS noise equivalent absorptions of approximately 3 ppm and 25 ppm, respectively. This noise is believed to be primarily due to pointing and intensity fluctuations in the probe laser. Discussion of the problem with associates of A. Boccara reinforced this hypothesis.[5]

VI. Frequency Response

The detector was placed in its PLDS configuration. The signal beam spot on the cavity input mirror was swept across the pump beam spot of radius 75 μm until a maximum deflection signal was observed. The signal was recorded as the modulation frequency was changed. The signal versus frequency curve, shown in Figure 5, consists of two plateaus corresponding to equations (1) and (2).

The signal versus frequency curve is of interest for two reasons. Firstly, it provides the multiplicative factors by which it is necessary to scale PLDS signals observed at various frequencies in order for comparison with equations (1) and (2) to take place. Secondly, when fit to equation (6),

$$\phi \propto \frac{1}{\sqrt{1+(\omega\tau)^2}} \tag{6}$$

where ϕ is the angular deflection, ω is the angular modulation frequency, and τ is the characteristic diffusion time, it yields a characateristic time of 9 ms, close to the expected value of 8 ms obtained from equation (3). The similarity between this experimentally obtained characteristic time and the characteristic time derived from theory suggests that the experiment is consistent with theory to at least some extent.

VII. Finite Probe Width

Equations (1), (2), and (4) assume an infinitesimal probe beam width. A program was written to determine the effect of finite probe width on deflection.

The results are shown in Figure 6. The deflections corresponding to various probe width to pump width ratios have been normalized to the deflection corresponding to an infinitesimal probe width. As can be seen from the figure, the deflection curve levels off when the probe width is approximately 2% of the pump width and falls approximately 15% when the probe width is raised to 70% of the pump width. This curve is of interest in that it provides a means of correcting deflection data collected with a probe beam of finite width.

VIII. Experimental PLDS Results

The detector was placed in its PLDS configuration. The pump and probe beam spots on the cavity input mirror were aligned vertically by adjusting the vertical position of the probe beam until a maximum signal was obtained. The probe beam spot was then moved horizontally across the pump beam spot. The signal strength was recorded as a function of the horizontal distance between the intensity maxima of the pump and probe beams, measured in turns of the fine adjustment knob of the Aerotech mirror mount used to guide the signal beam. The lineshape obtained in this manner closely resembled the lineshape described by equation (2).

Lineshapes for two positions on the cavity input mirror are shown in Figures 7 and 8. Comparison of these two figures with equation (2) yields absorptions of 15 ± 3 ppm and 96 ± 3 ppm, respectively. The wide disparity between the two

absorption values is a result of varying mirror cleanliness from day to day and from position to position, and of varying intrinsic absorption from position to position. Over the course of several months, lineshapes corresponding to absorptions as high as 600 ppm and as low as 5 ppm were obtained.

As can be seen in the figures, the experimental lineshape is asymmetrical in peak amplitude. This is a consequence of the angle between the signal and pump beams, and reverses when the angle is reversed.

Agreement between equations (1) and (2) was verified on two occasions. In each case, a lineshape was obtained for a single position on the cavity input mirror at a frequency above 250 Hz and a frequency below 8 Hz. The ratios of low frequency absorption values to high frequency absorption values were 1.06 ± 0.1 and 0.89 ± 0.1.

IX. Experimental PDDS Results

The detector was placed in its PDDS configuration. The procedure discussed in the previous section was followed. The lineshape obtained in this manner closely resembled the lineshape described by equation (4).

Lineshapes for two positions on the cavity input mirror are shown in Figures 9 and 10. Comparison of these two figures with equation (4) yields absorptions of 160 ± 25 ppm and 890 ± 25 ppm, respectively. Again, the wide disparity between these two values is a result of varying mirror cleanliness and varying

intrinsic absorption. Over the course of several weeks, lineshapes corresponding to absorptions between 900 ppm and 150 ppm were obtained.

As in the case of PLDS, peak asymmetry is a consequence of the angle between the signal and pump beams.

X. Calibration

Two methods of detector calibration are being investigated. The first of these is referred to as the calorimetry method. The cavity input mirror is encased in a holder comprised of three heat sensors. It is then exposed to the pump beam. The change in the voltage output of these sensors is proportional to the absorption. Unfortunately, the calorimetry measurements obtained so far have yielded absorption values larger than the values obtained from simultaneous deflection measurements by factors ranging from 10 to 30. This discrepancy is believed to be a result of inconsistencies in the calibration of the calorimetry holder.

The second of the two methods is referred to as the ultraviolet method. When a mirror is exposed to ultraviolet light, its absorption increases by approximately 60 to 100 ppm. An estimate of the mirror's total losses is obtained from the cavity decay time constant, as described earlier. An absorption estimate is simultaneously obtained by deflection measurement. The mirror is then exposed to ultraviolet light. Estimates of the total losses and absorption are reobtained. The change

in the total losses is equal to the change in the absorption. By comparison of the change in deflection to the change in total losses, it is possible to obtain a calibration. Although this method has been attempted, no reliable results have yet been obtained.

XI. Conclusion

The detector development stage of this project is now complete. Two stages remain incomplete. Firstly, the detector must be calibrated. Secondly, the data-taking procedure must be automated. When these two stages have been completed, an absorption testing facility will be assembled. Absorption maps of mirrors brought to this facility will be produced by computer-directed probe beam scans.

XII. Acknowledgments

The research discussed in this paper was conducted under the supervision of Dr. Fred Raab and with the assistance of LIGO graduate students Aaron Gillespie, Torrey Lyons, and Martin Regehr, and LIGO scientist Doug Jungwirth.

XIII. References

1. "Sensitive Photothermal Deflection Technique for Measuring Absorption in Optically Thin Media," N. Amer, A. Boccara, D. Fournier, and W. Jackson, *Optics Letters*, **5**, 377–379 (1980).

2. "Optical Distortion by Heated Windows in High-Power Laser Systems," M. Sparks, *J. Appl. Phys.*, **42**, 5029–5046 (1971).

3. "Photothermal Deflection Spectroscopy and Detection," N. Amer, A. Boccara, D. Fournier, and W. Jackson, *Applied Optics*, **20**, 1333–1344 (1981).

4. *The Art of Electronics*, W. Hill and P. Horowitz, 431–432 (1989).

5. A. Brillet and C. Nary-Man, private communication.

Figure 1: Theoretical PLDS Lineshape

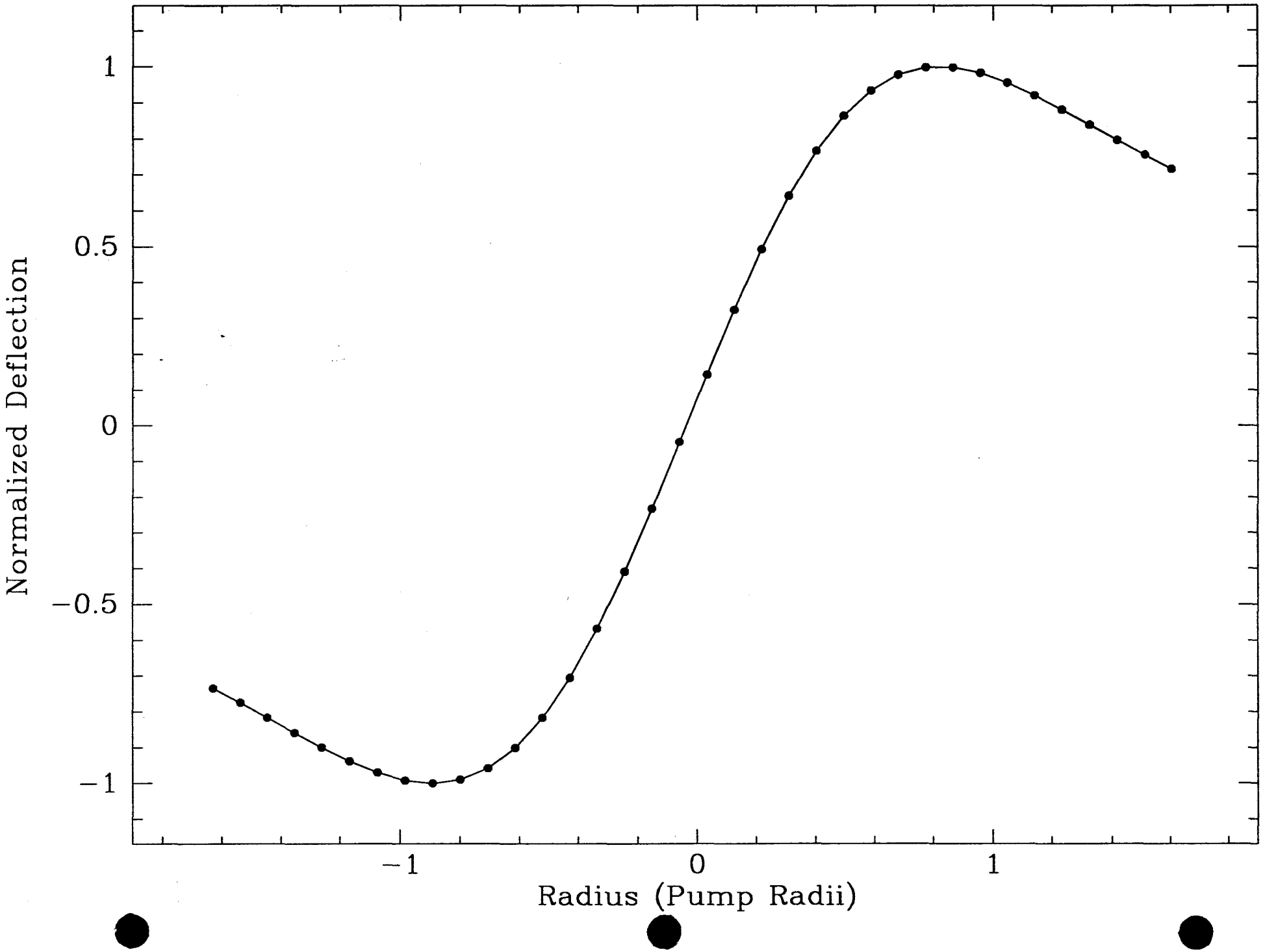

Figure 2: Theoretical PDDS Lineshape

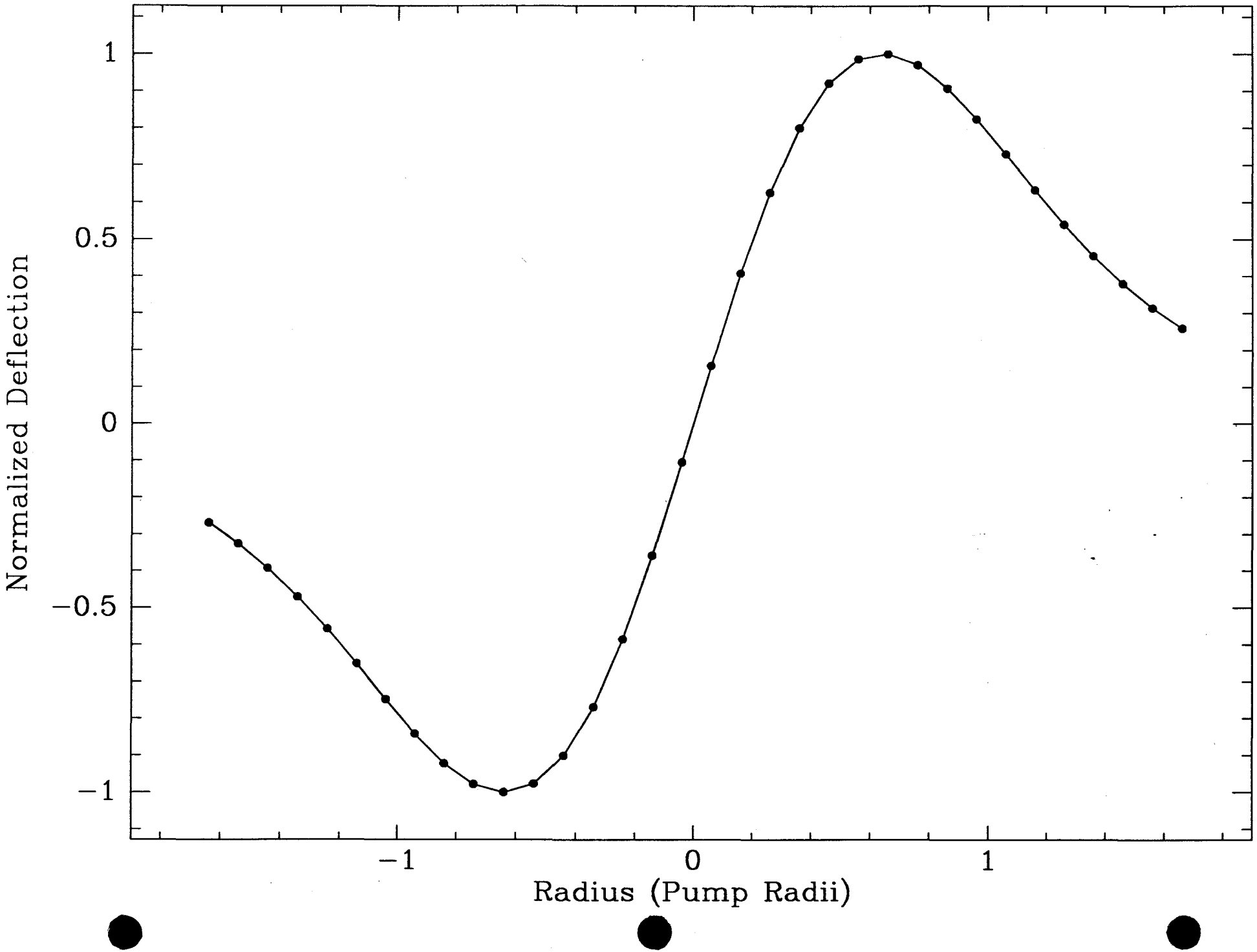

Figure 3: PLDS Detector Configuration

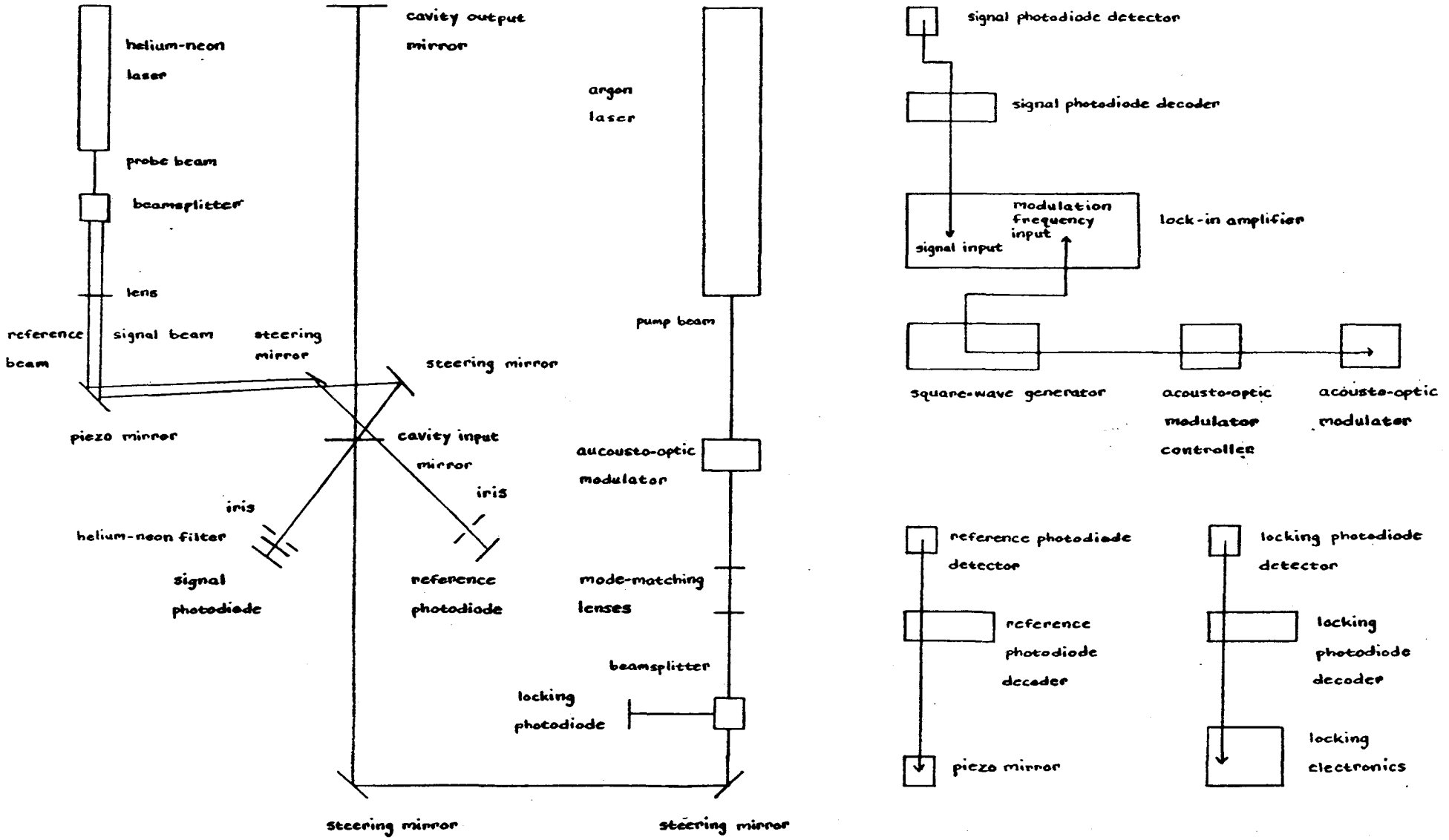

Figure 4: PDDS Detector Configuration

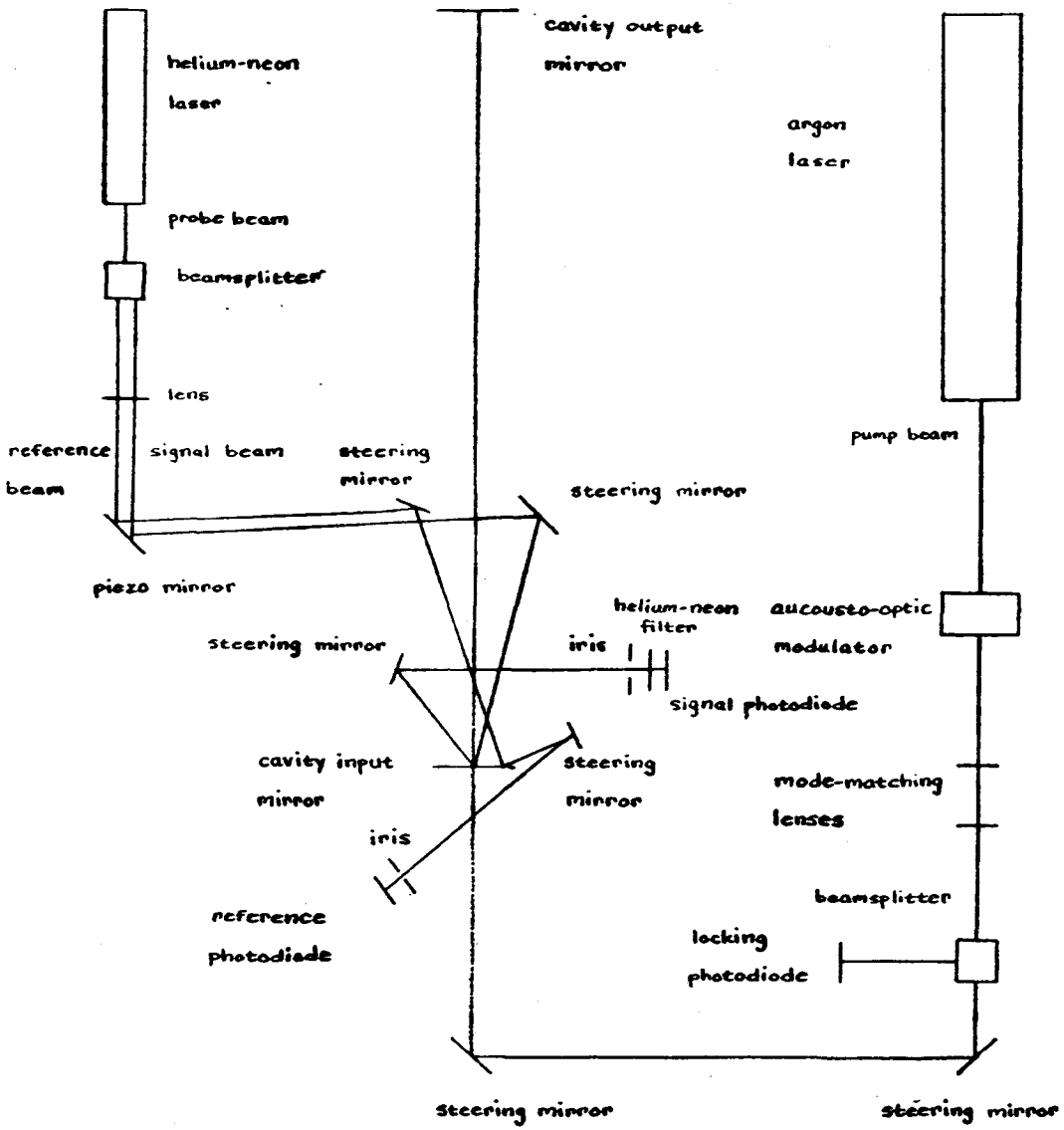

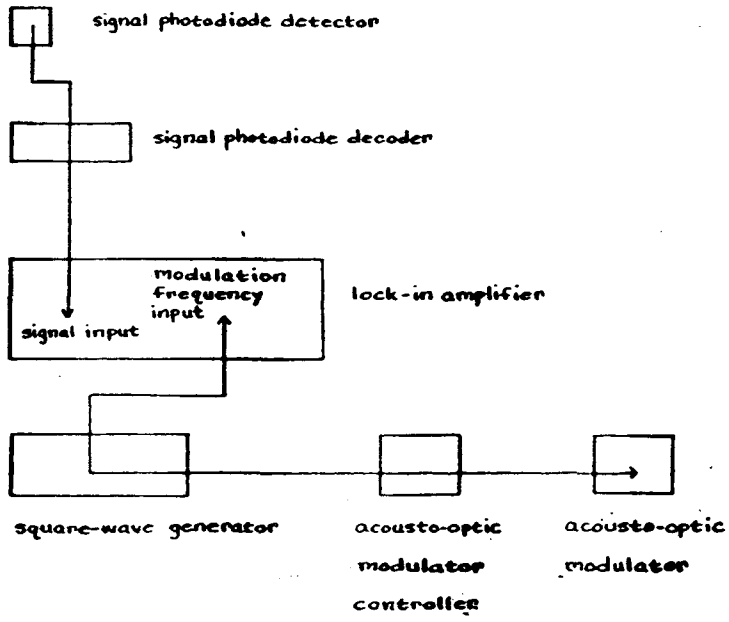

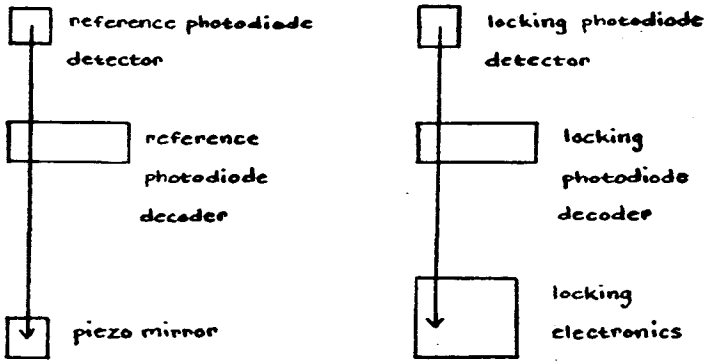

Figure 5: Detector Frequency Response

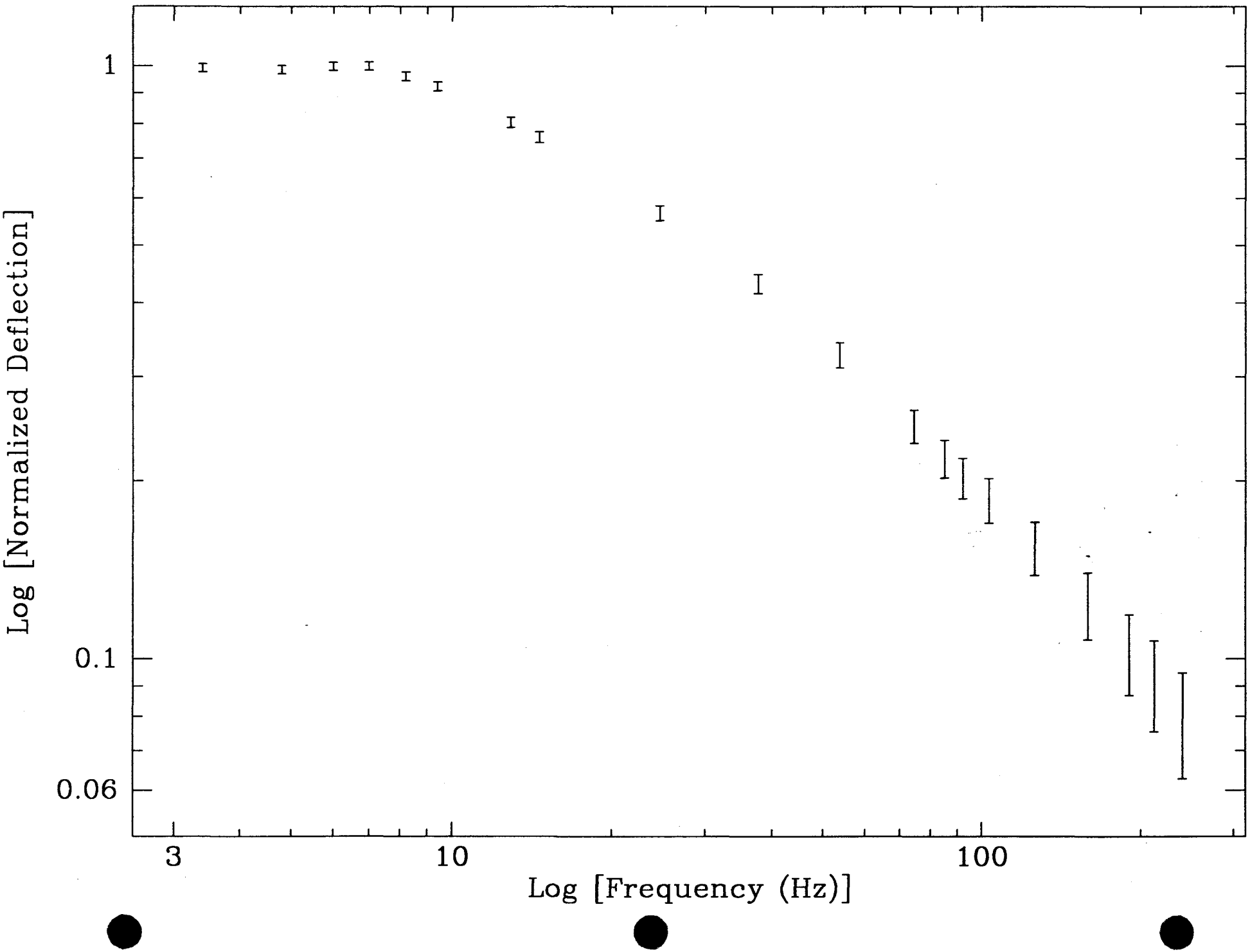

Figure 6: Detector Finite Probe Width Response

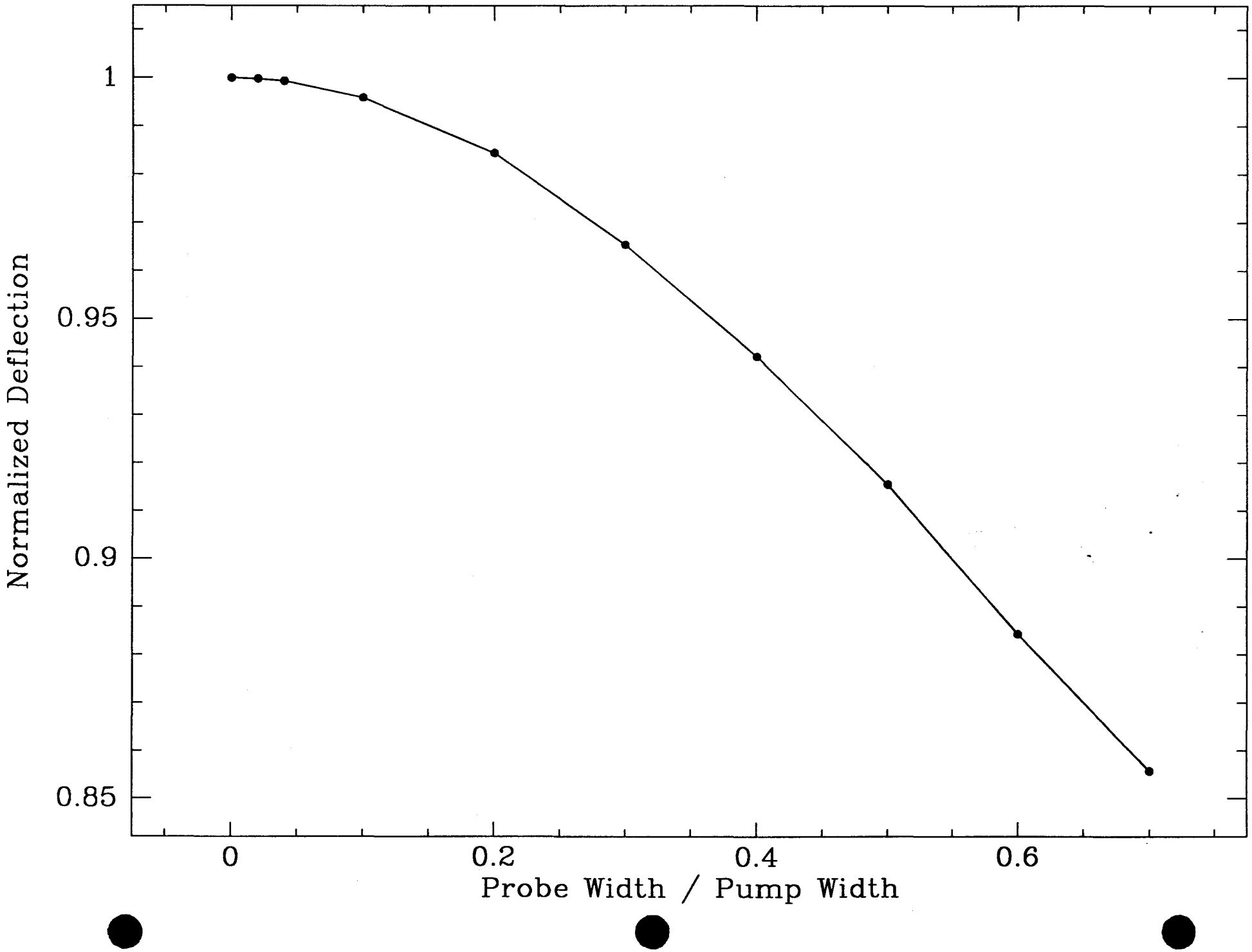

Figure 7: Experimental PLDS Lineshape (15 ppm)

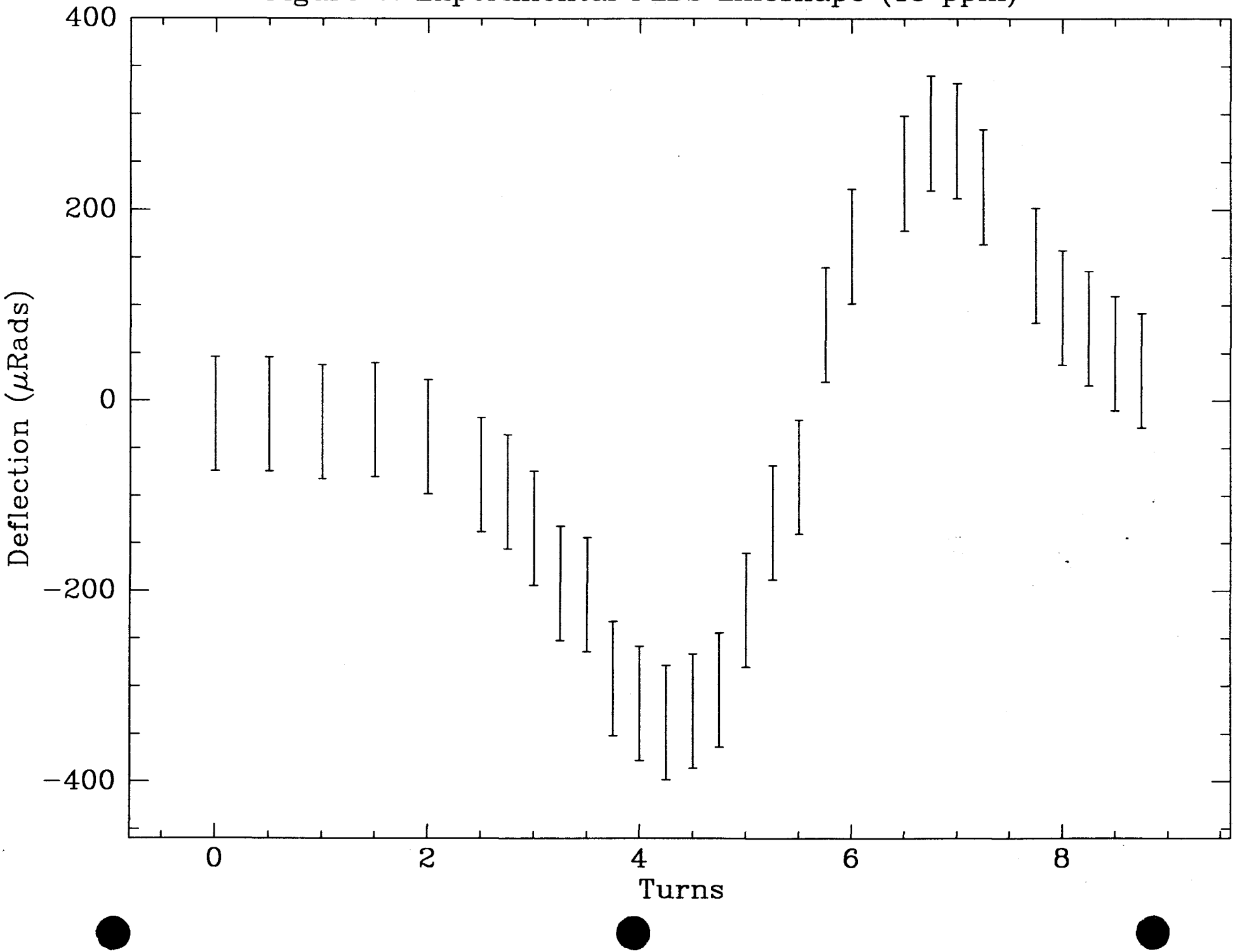

Figure 8: Experimental PLDS Lineshape (96 ppm)

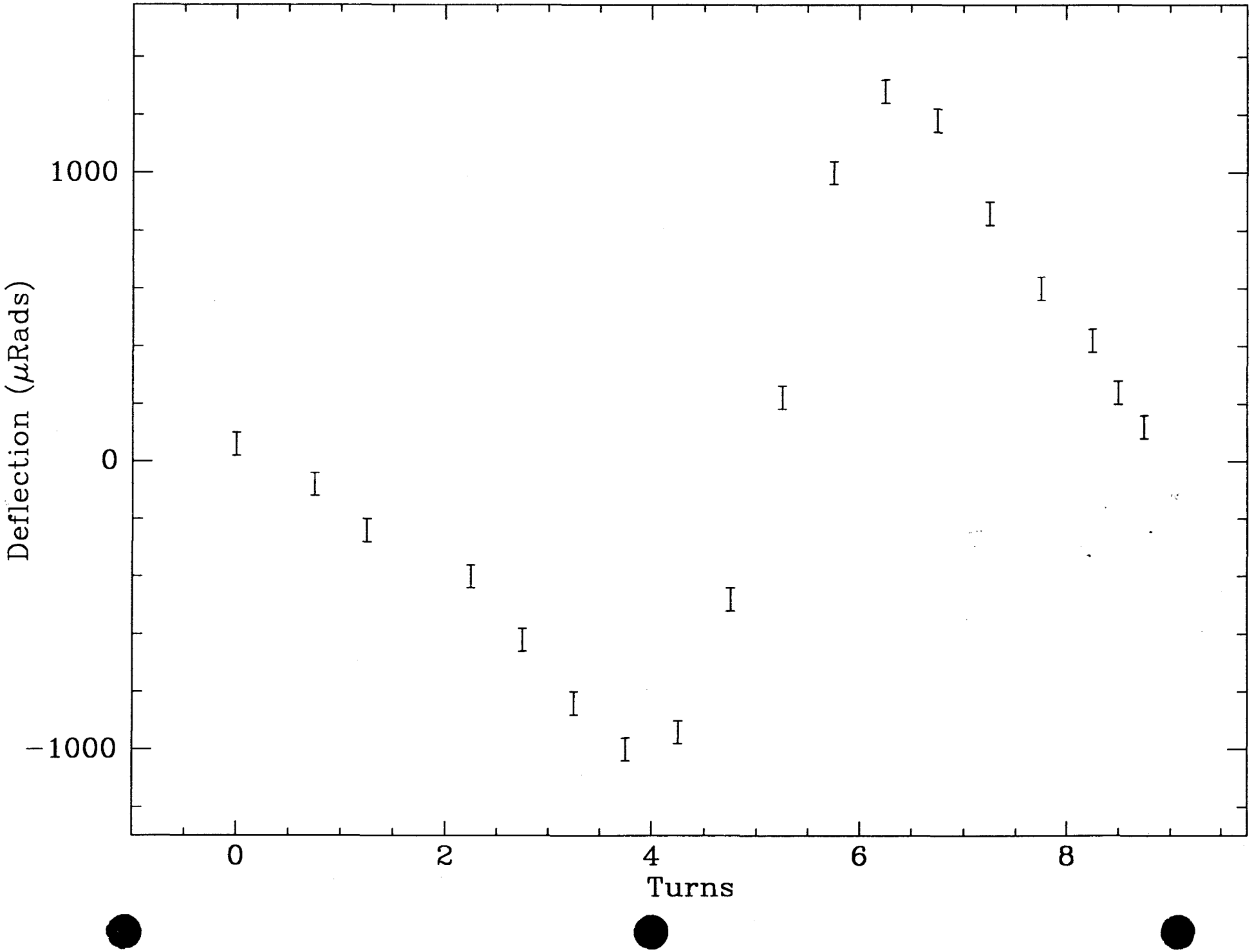

Figure 9: Experimental PDDS Lineshape (160 ppm)

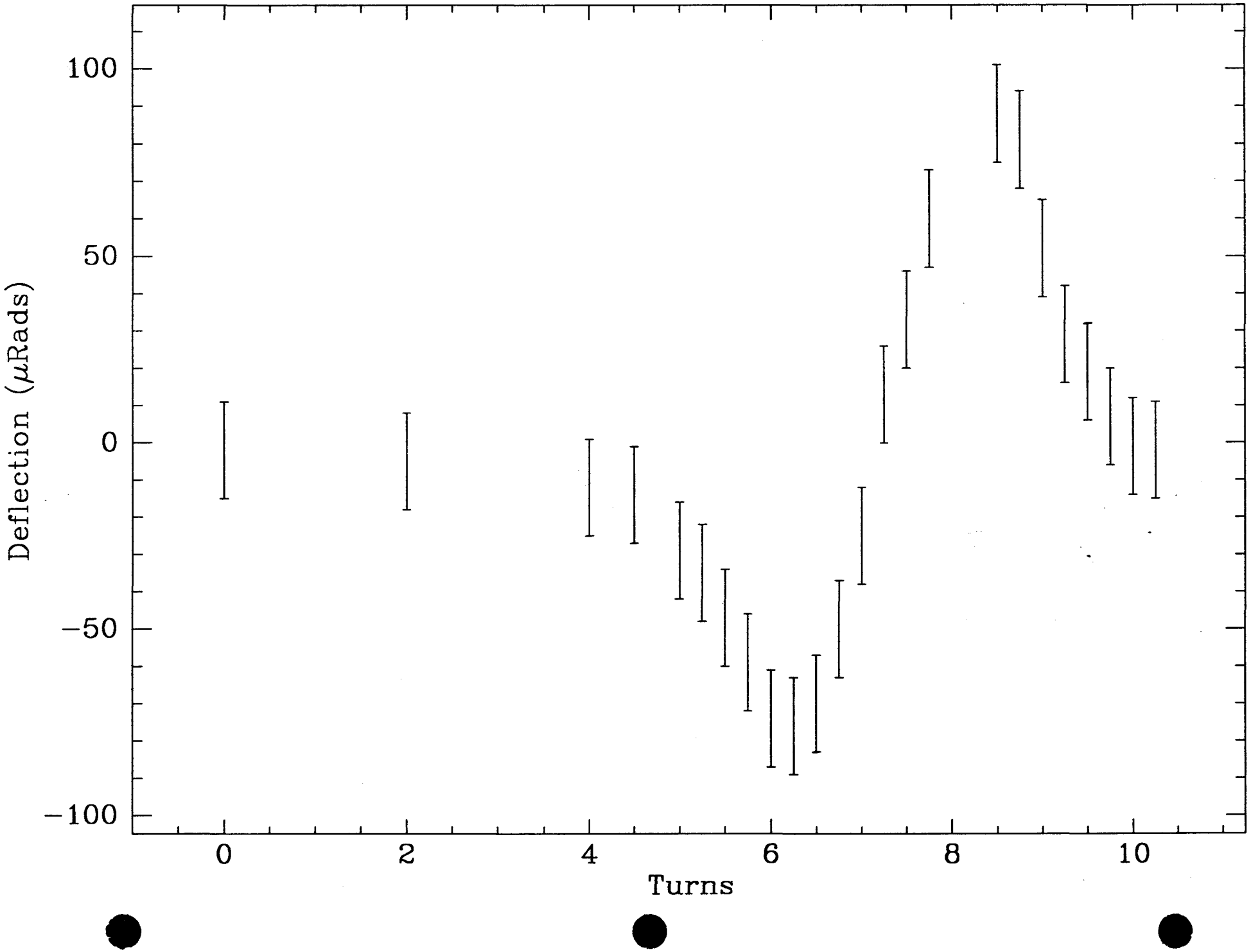

Figure 10: Experimental PDDS Lineshape (890 ppm)